Supporting Information

Corrosion Protection of Platinum-Based Electrocatalyst by Ruthenium Surface Decoration

Primož Jovanovič[*a,b], Marjan Bele[a], Martin Šala[b], Francisco Ruiz-Zepeda[a], Goran Dražić[a], Nataša Zabukovec Logar[c,d], Nejc Hodnik[*e], Miran Gaberšček*[a,f]

[a] *Department of Materials Chemistry, National Institute of Chemistry, Hajdrihova 19, SI-1000 Ljubljana, Slovenia*

[b] *Department of Analytical Chemistry, National Institute of Chemistry, Hajdrihova 19, SI-1000 Ljubljana, Slovenia*

[c] *Department of Inorganic Chemistry and Technology, National Institute of Chemistry, Hajdrihova 19, SI-1000 Ljubljana, Slovenia*

[d] *University of Nova Gorica, Vipavska 13, SI-5000 Nova Gorica, Slovenia*

[e] *Department of Catalysis and Chemical Reaction Engineering, National Institute of Chemistry, Hajdrihova 19, SI-1000 Ljubljana, Slovenia*

[f] *Faculty of Chemistry and Chemical Technology, University of Ljubljana, Večna pot 113, SI-1000 Ljubljana, Slovenia*

*Correspondence to: Primož Jovanovič (primoz.jovanovic@ki.si), Nejc Hodnik (nejc.hodnik@ki.si) and Miran Gaberšček (miran.gaberscek@ki.si)

S1 Preparation of $PtCu_3$/C and PtRuCu/C

The synthesis consists of the following steps.

1.1 Xero-gel preparation

To mix the reactants at the molecular level, 10 g of gelatine (GELATIN-B; Fluka, cat. No. 48722) and 0.9 g of cetyl-trimethyl-ammonium bromide (CTAB; Fluka, cat. No.52365) were dissolved in 250 mL of water at 60 °C while stirring, adding 12 g of copper acetate (Sigma-Aldrich; cat. No.25038) and 5 g of carbon black (VULCAN XC72R, CABOT). A mixture was obtained, which was homogenized while stirring for 20 min, followed by additional 10 min of stirring with a turbo stirrer Ultra Turax (15000 rpm). Afterward, the mixture was cooled to room temperature and left for 12 h. The obtained gel was freeze-dried with the use of liquid nitrogen and dried in vacuum. As found from the corresponding SEM images, thermal annealing of the gel precursor resulted in polydisperse Cu particle sizes ranging from a few hundred nm and all the way up to tens of microns. Even though this seems a very inconvenient way to prepare a precursor for the nanoparticles synthesis, the idea behind the preparation was to modify and stabilize the commercial Vulcan carbon support, while also providing enough copper for the next step of the synthesis – galvanic displacement reaction of platinum precursor salt.

1.2 Pyrolysis

In the second step, 2 g of dried xerogel was heated in a reductive atmosphere (H_2 (5%)/Ar, gas flow rate 50 mL/min) at a rate 10 °C/min to 800 °C for one h and cooled to room temperature. After having been heat treated, the composite of copper nanoparticles embedded in the porous matrix was appropriately grounded.

1.3 Platination

Platination of the composite was carried out using 0.21 g of potassium tetrachloroplatinate (Aldrich; cat. No. 323411), which had been dissolved in 25 mL of water solution while stirring. Addition of platinum precursor was performed in a two-step procedure. In the first step, 32 % of the total amount was added dropwise to 0.35 g of the composite of copper nanoparticles embedded in the carbon matrix. The obtained mixture was homogenized in ultrasonic bath stirred for 15 min after which the rest of the platinum precursor was added. The mixture was stirred continuously for 12 h. Afterwards, the solid part of the mixture was

separated from the liquid, washed 3 times with water and left to dry. The final composite material was obtained with annealing treatments.

1.4 Partial oxidation

The first heat treatment step involved partial oxidation of the platinized gel. This step was adapted to control the amount of carbon on catalyst nanoparticles. The composite material was first heat treated in an air atmosphere at a heating rate of 5 °C/min to 310 °C and then left at this temperature for 1 h. Such partial oxidation process uncovered nanoparticles buried within the support, as well as removed the so-called carbon film on the nanoparticles surface through a controlled carbon oxidation. Subsequently the less stable carbon was also removed - by sintering of very small particles to improve the corrosion resistance of the final $PtCu_3$/C catalyst due to very small particle sizes. A higher temperature in an oxidative atmosphere would result in a huge loss of carbon support due to severe carbon oxidation, as well as intense particle sintering.

1.5 Annealing

After partial oxidation, the composite material was heated at a rate of 10 °C/min to 750 °C for 30 min for solid solution formation. The sample was then cooled to 500 °C with a rate of 3 °C/min. After 30 minutes the temperature was dropped to 500^{o}C, and remained at that level for the next 12 hours. This step is necessary for the formation of the partially ordered crystal structure.

Ru decoration: After $PtCu_3$/C nanoparticles had been synthesized, Ru was added by dissolving a ruthenium(III) chloride precursor in a small volume of ethanol, mixed with the catalyst powder into a paste and left to evaporate. After subsequent annealing at 500 °C for 12 h under a reductive atmosphere (H_2/Ar, 5 %), a PtRuCu/C composite was obtained (Fig. 1). The content of Ru was 6 wt. %.

S2 X–ray powder diffraction analysis

X-ray powder diffraction patterns were collected at room temperature on a laboratory PANalytical X'Pert PRO diffractometer using Cu$K\alpha_1$ radiation (1.54060 Å). The samples were loaded into a flat disc-like sample holder. The XRPD data were collected in the 2θ range from 5 to 140º 2Θ in steps of 0.008º 2Θ with a total measurement time of 16 hours. The

qualitative and quantitative powder analysis of the collected XRPD pattern was performed using the Crystallographica Search-Match programs [1] and TOPAS V2.1 Rietveld refinement program [2].

In the Rietveld refinement of $PtCu_3$/C sample, the two Cu_3Pt phases with Fm-3m and Pm-3m symmetry were taken into account. In the Fm-3m phase, a random distribution of Cu and Pt over the (0,0,0) site was assumed. In the Pm3-m phase, Cu is occupying the (0,½,½) site and Pt (0,0,0) site. The diffraction peaks profiles were approximated using the Pseudo-Voigt approach. The refined parameters in the final cycle were 8 background polynomial parameters, zero shift, absorption correction, and for each phase lattice parameters, scale factors, microstrain and crystallite size. The refinement revealed an acceptable agreement between calculated and observed powder patterns; R_{wp} 12.1%.

In the Rietveld refinement of PtRuCu/C sample, the two Cu_3Pt phases with Fm-3m and Pm-3m symmetry and Ru phase were taken into account. In the Fm-3m phase, a random distribution of Cu and Pt over the (0,0,0) site was still assumed. Namely, a test refinement of Ru on Pt site did not lead to any improvement of the fit. In the Pm3-m phase, Cu was still assumed to occupy the (0,½,½) site and Pt (0,0,0) site. Additionally, Ru occupancy was taken into account in refinement at the (0,0,0) site, which revealed that a small fraction of Pt could be replaced by Ru (4(2)%). The diffraction peaks profiles were approximated using Pseudo-Voigt approach. The refined parameters in the final cycle were 8 background polynomial parameters, zero shift, absorption correction, for Pm-3m phase the Ru/Pt occupancy and for each phase lattice parameters, scale factors, microstrain and crystallite size. The refinement revealed an acceptable agreement between calculated and observed powder patterns; R_{wp} 11.8%.

Results of Rietveld analysis:

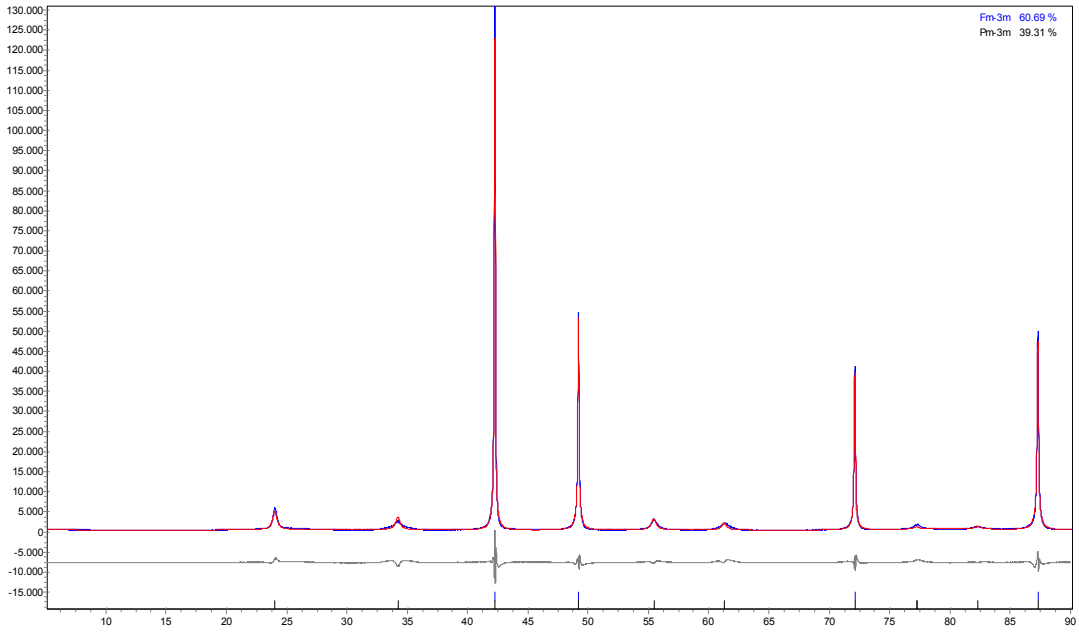

Figure S1: Observed (blue), calculated (red) and difference (gray) curves for $PtCu_3$/C analogue obtained by program TOPAS V2.1.

Table S1: Crystal data and final refinement parameters for $PtCu_3$/C:

Phases' names	(1) Cu_3Pt-Fm-3m and (2) Cu_3Pt-Pm-3m
Unit cell (1)	cubic; Fm-3m; a(Å)=3.69974(3)
Unit cell (2)	cubic; Pm-3m; a(Å)=3.70097(8)
Crystallite size (1)	180(9) nm
Crystallite size (1)	11.6(7) nm
R_p(%)	8.90
R_{wp}(%)	12.27
R_{ex}(%)	2.82
Profile function	Pseudo-Voigt approach
Background function	polynomial Chebychev, order 8

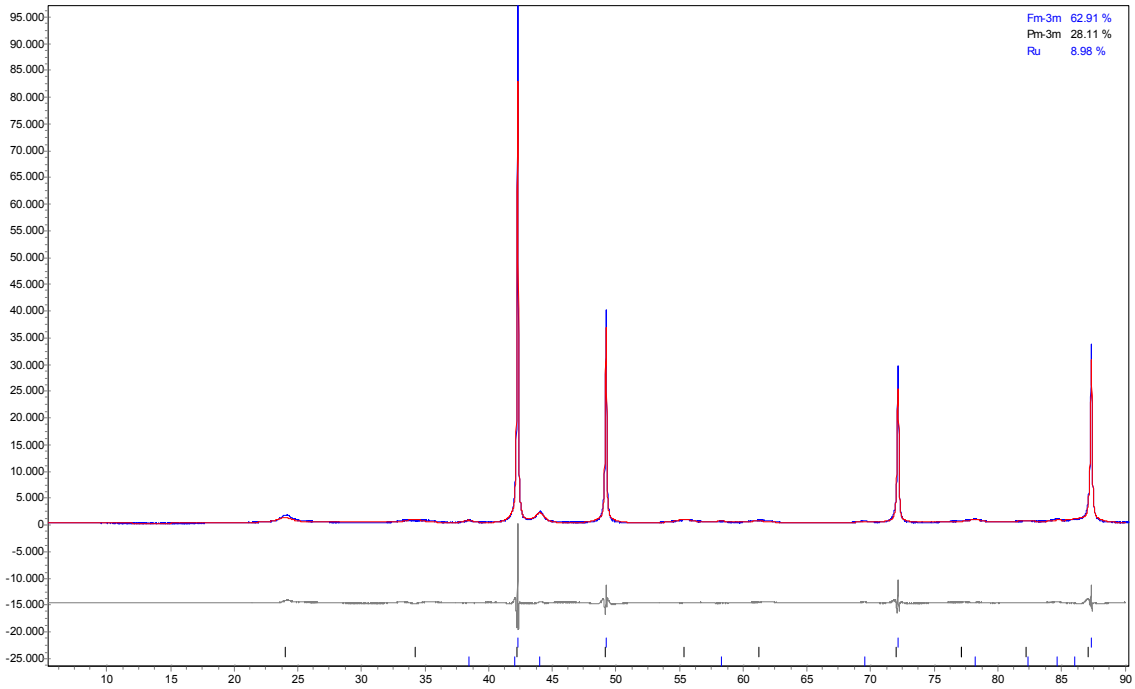

Figure S2: Observed (blue), calculated (red) and difference (gray) curves for $PtCu_3$/C analogue obtained by program TOPAS V2.1.

Table S2: Crystal data and final refinement parameters for PtRuCu/C:

Phases' names	(1) Cu_3Pt-Fm-3m, (2) Cu_3Pt-Pm-3m and (3) Ru
Unit cell (1)	cubic; Fm-3m; a(Å)=3.69911(7)
Unit cell (2)	cubic; Pm-3m; a(Å)=3.7059(1)
Unit cell (3)	hexagonal; $P6_3/mmc$; a(Å)=2.7019(4), c(Å)=4.297(1)
Crystallite size (1)	161(9) nm
Crystallite size (1)	10.3(5) nm
Crystallite size (1)	12.6(8) nm
R_p(%)	9.47
R_{wp}(%)	12.14
R_{ex}(%)	3.18
Profile function	Pseudo-Voigt approach
Background function	polynomial Chebychev, order 8

Table S3: XRD Data collection parameters.

Instrument	PANalytical X'Pert PRO MPD
Radiation	CuKα1 (1.540596 Å)
Temperature	293(1) K
Tension, current	45 kV, 40 mA
Specimen	Flat-plate
Mask	10 mm
Divergence slit	10 mm
Scatter slit	10 mm
Soller slit (primary)	0.01 rad
Soller slit (secondary)	0.01 rad
Monochromator	Ge, Johansson type
Detector	Full range
Range of 2θ	5–140
Step width	0.008
Time per step	432 s

S3 Transmission electron microscopy analysis:

As prepared analogues:

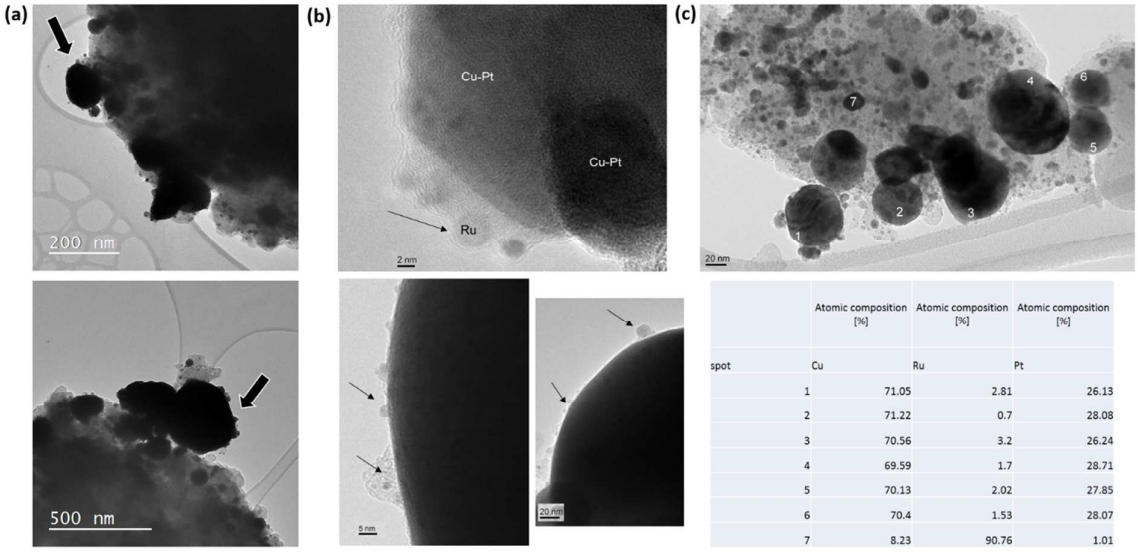

spot	Atomic composition [%] Cu	Atomic composition [%] Ru	Atomic composition [%] Pt
1	71.05	2.81	26.13
2	71.22	0.7	28.08
3	70.56	3.2	26.24
4	69.59	1.7	28.71
5	70.13	2.02	27.85
6	70.4	1.53	28.07
7	8.23	90.76	1.01

Figure S3: (a) TEM images of as prepared Ru analogue. The arrows point to regions with particles decorated with small nanoparticles. (b) Surface of CuPt particles decorated with Ru nanoparticles. (c) Energy dispersive X ray analysis of as prepared Ru analogue and the corresponding quantification in tabular form.

After electrochemical activation cycles:

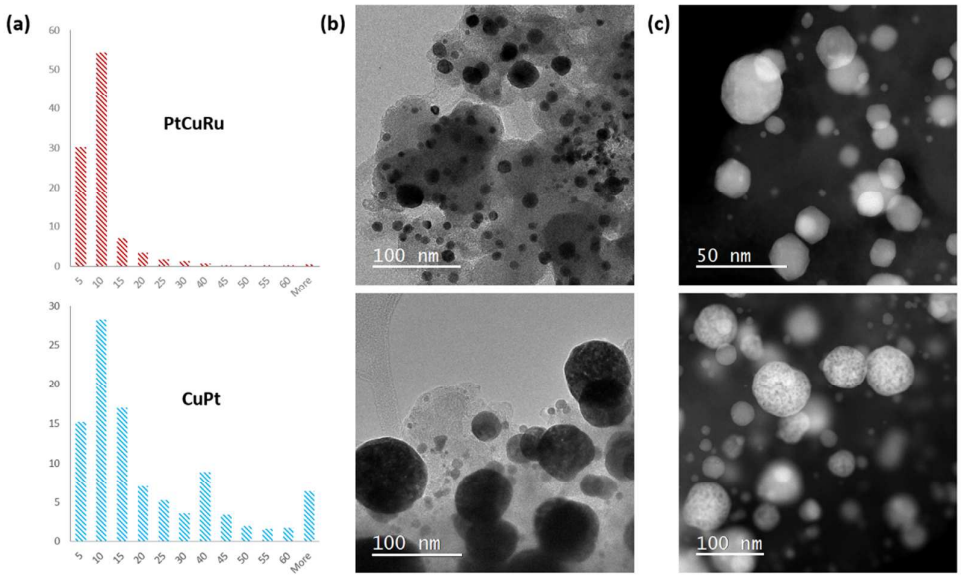

Figure S4: Comparision of Ru and Pt analogues after electrochemical activation. (a) Histograms of particle size distribution. (b) TEM images and (c) STEM HAADF images. In the Ru analogue, we have observed that the average size is smaller (a,b), and that less porous particles formed (c) due to the effect of corrosion protection.

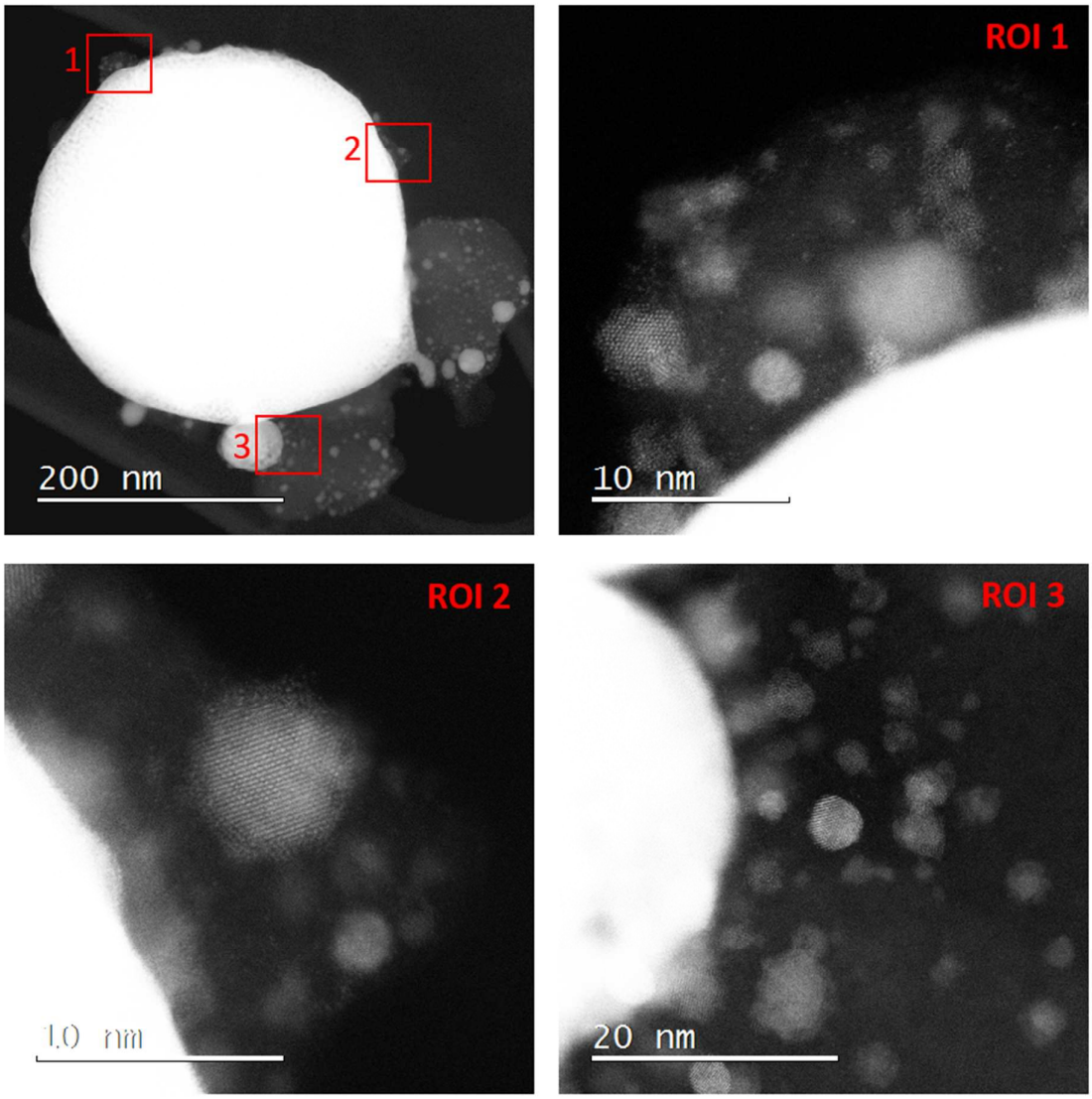

Figure S5: STEM HAADF images of a Ru analogue after the electrochemical activation pretreatment. Three regions of interest (ROIs) are selected from the surface of the larger CuPt particle and analyzed in further detail. The larger CuPt particle is decorated by small Ru nanoparticles.

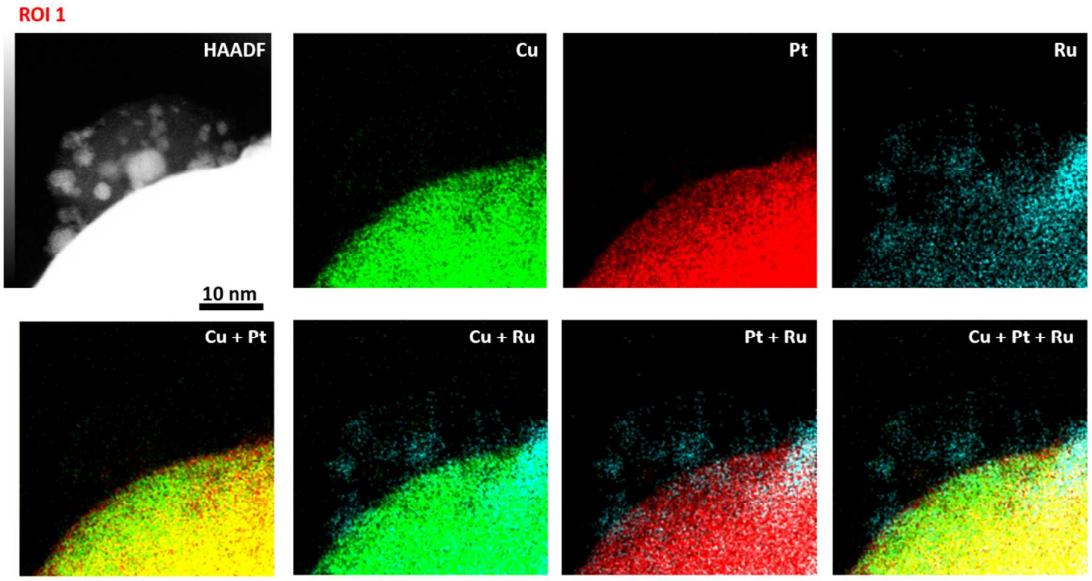

Figure S6: ROI 1 from Figure S5. Energy dispersive X ray maps of Ru analogue after the electrochemical activation pretreatment. In this region, Ru nanoparticles on carbon are decorating the surface of a larger CuPt particle. Pt skin can be observed at the surface of the CuPt particle.

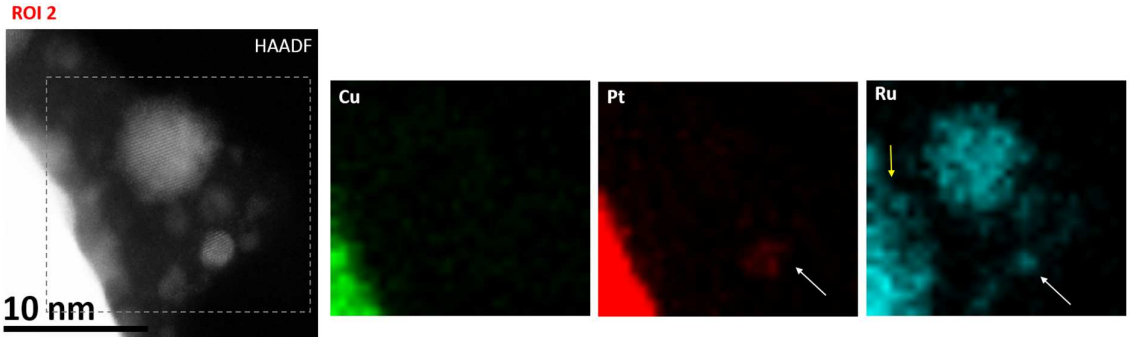

Figure S7: ROI 2 from Figure S5. Energy dispersive X ray maps of Ru analogue after electrochemical activation pretreatment. Notice in the Ru chemical map, aside from the bigger Ru particle, the signal from smaller particles located on the surface of the larger CuPt particle (yellow arrow). Additionally, a core-shell Ru@Pt nanoparticle is detected (white arow).

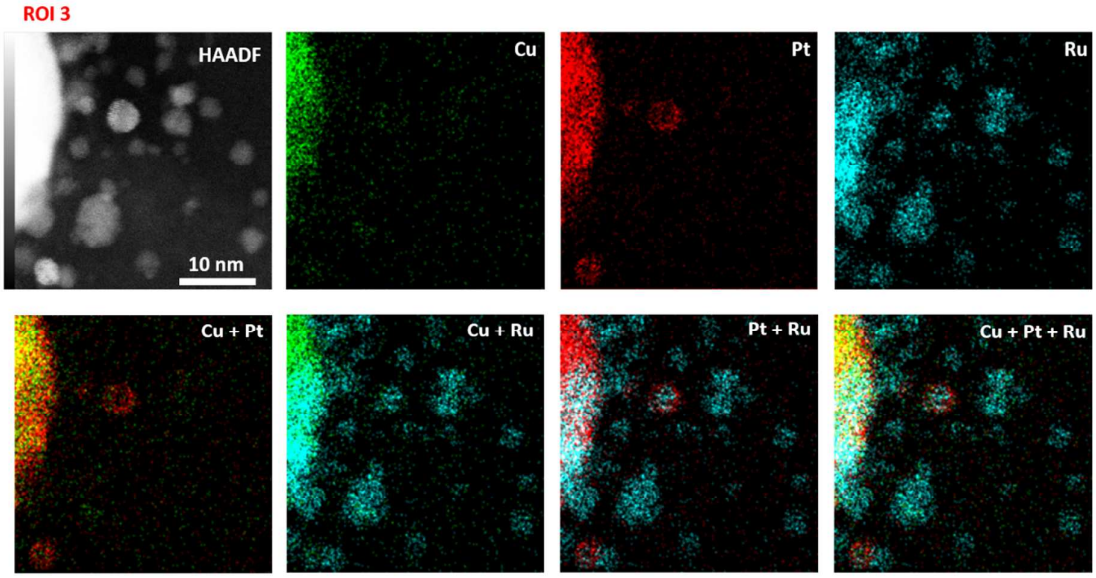

Figure S8: ROI 3 from Figure S5. Energy dispersive X ray maps of Ru analogue after the electrochemical activation pretreatment. In this region, aside from the multiple Ru nanoparticles detected, some core-shell Ru@Pt nanoparticles are observed on the surface of the CuPt nanoparticle.

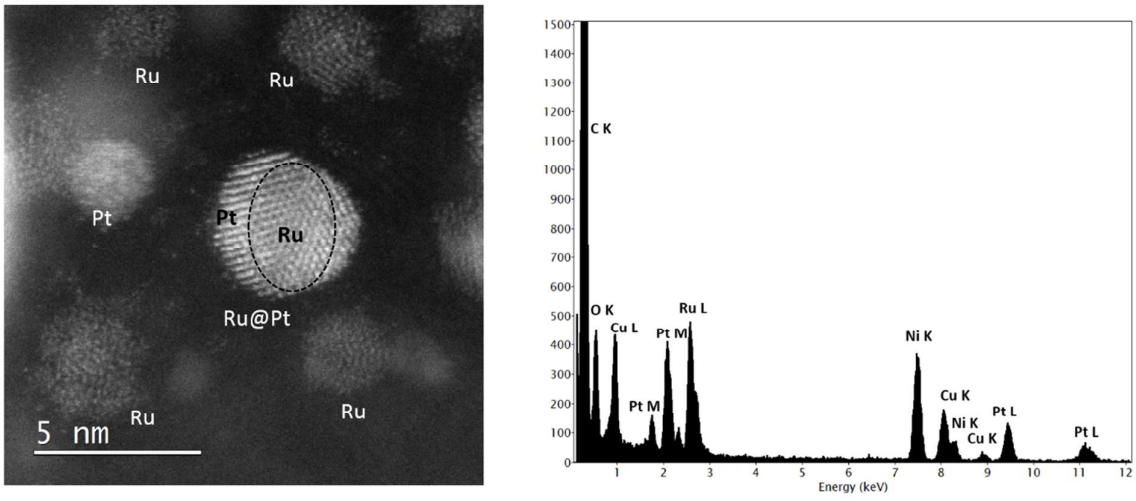

Figure S9: STEM HAADF image of a core-shell Ru@Pt particle along with other Ru and Pt particles. The image is taken from a section of ROI 3, where few small paticles are located at the surface of the larger CuPt particle. Next to the image, an EDX signal shows the presence of Cu, Pt, and Ru. A Niquel grid was used for the TEM sample analyis in order to aovid any signal peak overlapping with the present elements.

S4: Electrochemical flow cell coupled to inductively plasma mass spectrometry measurements

A replica of BASi electrochemical flow cell (Cross-Flow Cell Kit MW-5052) made of TECAPEEK material was coupled with an Agilent 7500ce ICP-MS instrument (Agilent Technologies,Palo Alto, USA) equipped with a MicroMist glass concentric nebulizer and a Peltier-cooled Scott-type double-pass quartz spray chamber. A forward radio frequency power of 1500 W was used with the following Ar gas flows: carrier 0.85 $Lmin^{-1}$, makeup 0.28 $Lmin^{-1}$, plasma 1 $Lmin^{-1}$, and cooling 15 $Lmin^{-1}$. $HClO_4$ (0.1 $molL^{-1}$, Aldrich 70%, 99.999% trace metals basis) carrier solution for the electrochemical experiments was pumped at 263 $\mu Lmin^{-1}$ by using a peristaltic pump into the EC flow cell and then directly into the nebulizer of the ICP-MS. The carrier solution and electrochemical cell were electrically grounded with respect to the ICP-MS to minimize the possibility of ICP-MS response spikes from static charging at the peristaltic pump rollers. The ICPMS was tuned for high sensitivity to obtain the best possible signal-to-noise ratio for the measurements. The suspension was cast dropped by micropipette over one of the GC electrodes and stabilized by a 5 µL of Nafion® (5 wt. % water suspension) diluted by isopropanol (1/50). Second GC electrode was used as a counter electrode. The orientation of the working (WE) and counter (CE) electrode was adjusted so that WE was placed after CE in the direction of the electrolyte flow. Ag/AgCl was used as a reference electrode.

S4.1: Cu and Pt dissolution

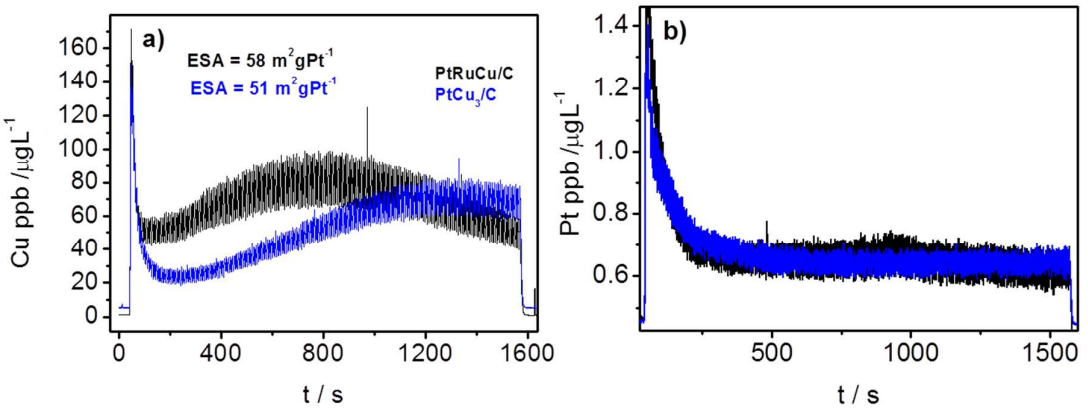

Figure S10: a) Copper and b) platinum dissolution profiles of Ru and non-Ru analogue during potential cycling from 0.05 V to 1.2V vs. RHE with a scan rate of 300 mVs^{-1}.

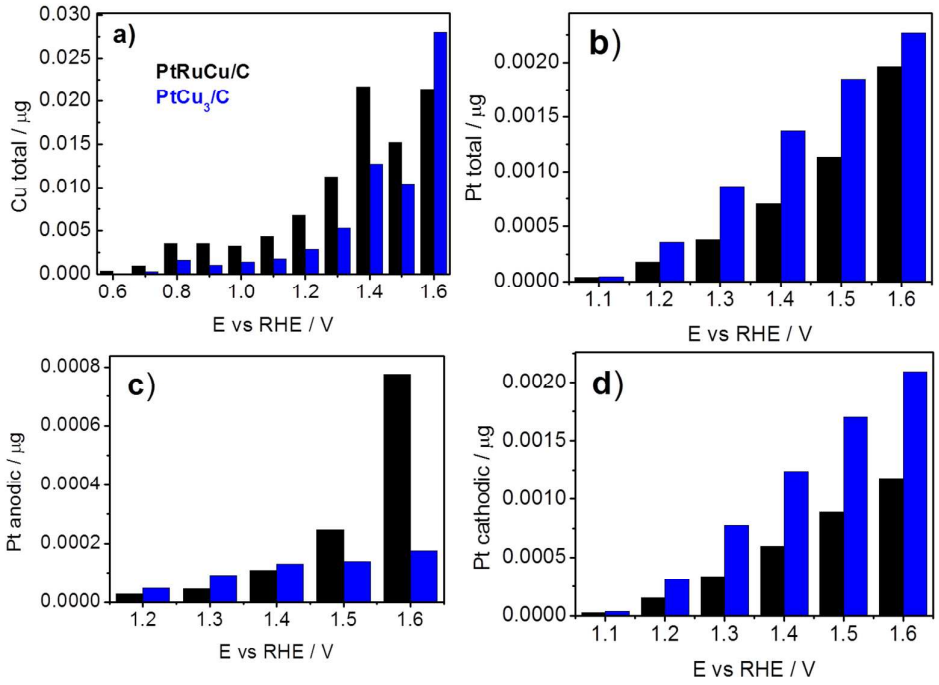

Figure S11: a) Cu and b) Pt dissolution amounts under different upper potential limits. Pt dissolution profiles were separately integrated to resolve c) anodically and d) cathodically dissolved Pt.

S4.3: Ru dissolution

Dissolution of ruthenium has been investigated by using the same highly sensitive analytics as in the present work. The dissolution process was monitored in a wide potential window which enabled the elucidation od Ru corrosion; the interested reader is deployed to refs. [3,4]. Ru dissolution will only be described briefly for the case of Pt-Cu-Ru/C sample. In general Ru dissolution, as is the case with Pt, is transient by nature, meaning it is dependent on the formation/reduction of surface oxides. The corresponding reactions are listed in Table S4 and were adapted from ref. [3]. In the low potential region (upper potential limits of 0.9 to 1.1 V) Ru dissolves due to the formation of RuO_2 (peak 2-Fig. S.3.3.1a) and reduction of several compounds (peak 1 and 4). In the high potential region (above the upper potential limit of 1.3 vs. RHE) anodic dissolution due to the formation of unstable Ru(>IV) is the predominant corrosion process (peak 3-Fig. S.3.3.1b).

Table S4: Thermodynamic Nernst equations describing Ru dissolution phenomena

Peak	Dissolution Process	Reaction	Potential or E_o =
1	Transient dissolution: (reduction of "irreversible" RuO_x)	$RuO_x + 2xH^+ + 2xe^- = Ru + xH_2O$	0.2 – 0.05 V vs. RHE
2	Transient dissolution: (oxidation)	$Ru_2O_3 + H_2O = 2RuO_2 + 2H^+ + 2e^-$	0.937 V – 0.0591pH
3	Anodic oxidation with subsequent chemical dissolution Or Direct anodic dissolution (oxidation)	$RuO_2 + 2H_2O = RuO_4 + 4H^+ + 4e^-$ $RuO_4 + H_2O = H_2RuO_{5(aq)}$ $RuO_2 + 3H_2O = H_2RuO_{5(aq)} + 4H^+ + 4e^-$	1.387 V – 0.0591pH 1.400 - 0.0591pH + $0.0148\log(H_2RuO_5)$
4	Transient dissolution: (reduction of "reversible" RuO_x) with subsequent direct anodic dissolution	$2RuO_2 + 2H^+ + 2e^- = Ru_2O_3 + H_2O$ $Ru_2O_3 + 6H^+ + 6e^- = 2Ru + 3H_2O$ $Ru = Ru^{2+} + 2e^-$	0.937 V – 0.0591pH 0.738 V – 0.0591pH 0.455 V + $0.0295\log(Ru^{2+})$

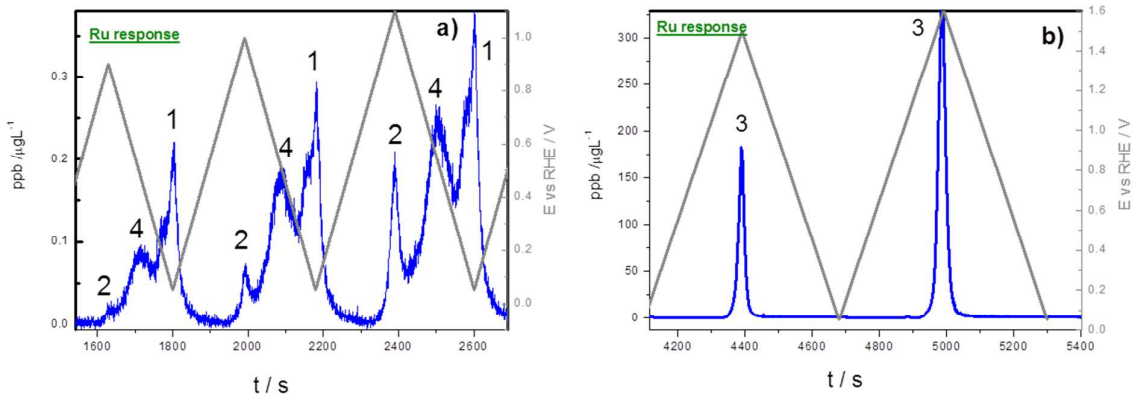

Figure S12: Ru dissolution profiles during potentiodynamic cycling till a) 0.9, 1.0, 1.1 V and b) during potentiodynamic cycling till 1.5 and 1.6 V vs. RHE.

S4.4: Cyclovoltammetry in the OER region

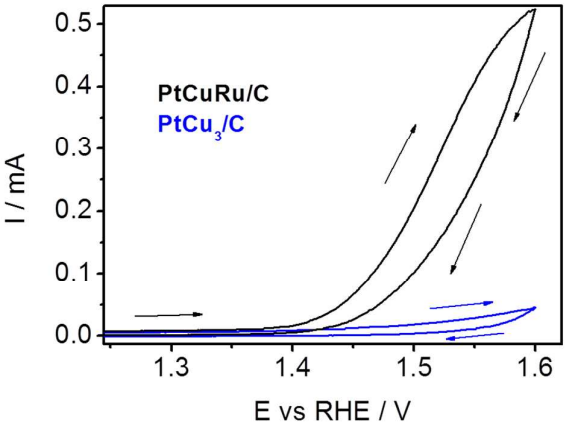

Figure S13: Cyclovoltammetric response when cycling till 1.6 V for the two analogues in an EFC configuration.

S5: Thin film rotating disc electrode (TF-RDE) measurements

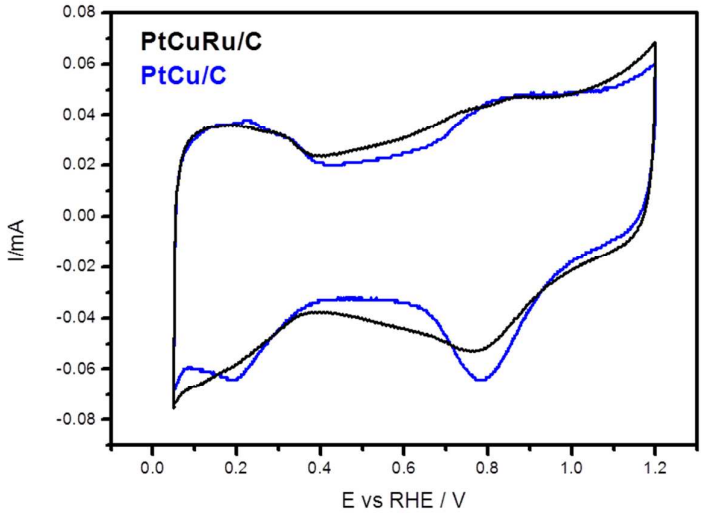

Figure S14: Cyclovoltammetric response when cycling till 1.2 V (20 mVs^{-1}) for the two analogues in a TF-RDE configuration. Cyclovoltammograms were recorded after 200 »activation cycles« from 0.05 V to 1.2V vs. RHE with a scan rate of 300 mVs^{-1}.

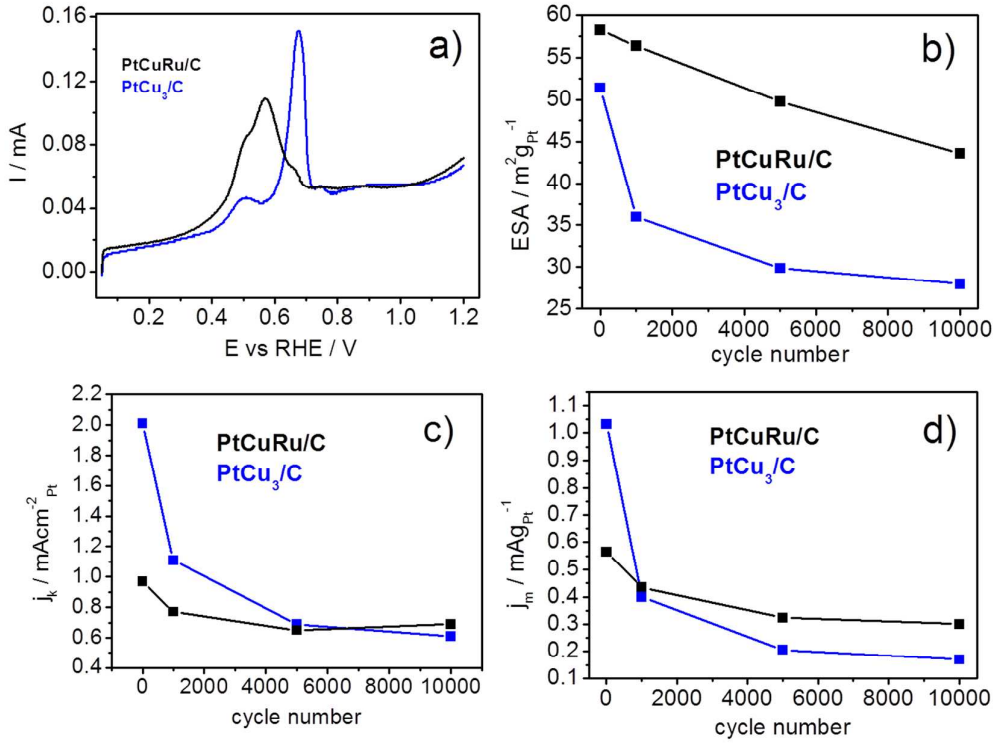

Figure S15:a) CO stripping voltammetric response (20 mVs-1) recorded after 200 »activation cycles« from 0.05 V to 1.2V vs RHE with a scan rate of 300 mVs^{-1}. b-d) Results of the TF-RD start/stop degradation protocol consisted of 10 000 cycles between 0.4-1.4 V vs. RHE.; Changes of b) ESA, c) specific ORR activity and d) mass ORR activity during degradation,

References

[1] Crystallographica Search-Match, version 2,1,1,0, Oxford Cryosystems, UK, 2003, (n.d.).

[2] TOPAS V2.1, Users Manual, Bruker AXS, Karlsruhe, Germany, 2000, (n.d.).

[3] N. Hodnik, P. Jovanovič, A. Pavlišič, B. Jozinović, M. Zorko, M. Bele, V.S. Šelih, M. Šala, S. Hočevar, M. Gaberšček, New Insights into Corrosion of Ruthenium and Ruthenium Oxide Nanoparticles in Acidic Media, J. Phys. Chem. C. 119 (2015) 10140–10147. doi:10.1021/acs.jpcc.5b01832.

[4] P. Jovanovič, V.S. Šelih, M. Šala, S. Hočevar, F. Ruiz-Zepeda, N. Hodnik, M. Bele, M. Gaberšček, Potentiodynamic dissolution study of PtRu/C electrocatalyst in the presence of methanol, Electrochim. Acta. 211 (2016) 851–859. doi:10.1016/j.electacta.2016.06.109.